









# Spectroscopic near-infrared photodetectors enabled by strong light–matter coupling in (6,5) single-walled carbon nanotubes

Cite as: J. Chem. Phys. **153**, 201104 (2020); <https://doi.org/10.1063/5.0031293>

Submitted: 29 September 2020 . Accepted: 11 November 2020 . Published Online: 30 November 2020

 Andreas Mischok,  Jan Lüttgens, Felix Berger, Sabina Hillebrandt,  Francisco Tenopala-Carmona,  Seonil Kwon,  Caroline Murawski,  Bernhard Siegmund,  Jana Zaumseil, and  Malte C. Gather

## COLLECTIONS

Paper published as part of the special topic on [Polariton Chemistry: Molecules in Cavities and Plasmonic MediaPOM2020](#)



View Online



Export Citation



CrossMark

## ARTICLES YOU MAY BE INTERESTED IN

[Nano-second exciton-polariton lasing in organic microcavities](#)

Applied Physics Letters **117**, 123302 (2020); <https://doi.org/10.1063/5.0019195>

[Nuclear magnetic resonance spin-lattice relaxation of lithium ions in aqueous solution by NMR and molecular dynamics](#)

The Journal of Chemical Physics **153**, 184502 (2020); <https://doi.org/10.1063/5.0026450>

[Quantum Monte Carlo benchmarking of large noncovalent complexes in the L7 benchmark set](#)

The Journal of Chemical Physics **153**, 194113 (2020); <https://doi.org/10.1063/5.0026275>



**New**

## Your Qubits. Measured.

Meet the next generation of quantum analyzers

- Readout for up to 64 qubits
- Operation at up to 8.5 GHz, mixer-calibration-free
- Signal optimization with minimal latency

Find out more



# Spectroscopic near-infrared photodetectors enabled by strong light–matter coupling in (6,5) single-walled carbon nanotubes

Cite as: J. Chem. Phys. 153, 201104 (2020); doi: 10.1063/5.0031293

Submitted: 29 September 2020 • Accepted: 11 November 2020 •

Published Online: 30 November 2020



View Online



Export Citation



CrossMark

Andreas Mischok,<sup>1,a)</sup> Jan Lüttgens,<sup>2</sup> Felix Berger,<sup>2</sup> Sabina Hillebrandt,<sup>1</sup>  
Francisco Tenopala-Carmona,<sup>1</sup> Seonil Kwon,<sup>1</sup> Caroline Murawski,<sup>1,3</sup> Bernhard Siegmund,<sup>4</sup>  
Jana Zaumseil,<sup>2,b)</sup> and Malte C. Gather<sup>1,5,c)</sup>

## AFFILIATIONS

<sup>1</sup>Organic Semiconductor Centre, SUPA, School of Physics and Astronomy, University of St Andrews, North Haugh, St Andrews KY16 9SS, United Kingdom

<sup>2</sup>Institute for Physical Chemistry and Centre for Advanced Materials, Universität Heidelberg, 69120 Heidelberg, Germany

<sup>3</sup>Kurt-Schwabe-Institut für Mess- und Sensortechnik Meinsberg e.V., Kurt-Schwabe-Str. 4, 04736 Waldheim, Germany

<sup>4</sup>Heliatek GmbH, Treidlerstraße 3, 01139 Dresden, Germany

<sup>5</sup>Centre for Nanobiophotonics, Department of Chemistry, Greinstr. 4-6, 50939 Köln, Germany

**Note:** This paper is part of the JCP Special Topic on Polariton Chemistry: Molecules in Cavities and Plasmonic Media.

<sup>a)</sup> Author to whom correspondence should be addressed: [am470@st-andrews.ac.uk](mailto:am470@st-andrews.ac.uk)

<sup>b)</sup> [zaumseil@pci.uni-heidelberg.de](mailto:zaumseil@pci.uni-heidelberg.de)

<sup>c)</sup> [mcg6@st-andrews.ac.uk](mailto:mcg6@st-andrews.ac.uk)

## ABSTRACT

Strong light–matter coupling leads to the formation of mixed exciton–polariton states, allowing for a rigorous manipulation of the absorption and emission of excitonic materials. Here, we demonstrate the realization of this promising concept in organic photodetectors. By hybridizing the  $E_{11}$  exciton of semiconducting (6,5) single-walled carbon nanotubes (SWNTs) with near-infrared cavity photons, we create spectrally tunable polariton states within a photodiode. In turn, we are able to red-shift the detection peak that coincides with the lower polariton band. Our photodiodes comprise a metal cavity to mediate strong coupling between light and SWNTs and utilize P3HT and PC<sub>70</sub>BM as the electron donor and acceptor, respectively. The diodes are formed either via mixing of SWNTs, P3HT, and PC<sub>70</sub>BM to create a bulk heterojunction or by sequential processing of layers to form flat heterojunctions. The resulting near-infrared sensors show tunable, efficient exciton harvesting in an application-relevant wavelength range between 1000 nm and 1300 nm, with optical simulations showing a possible extension beyond 1500 nm.

Published under license by AIP Publishing. <https://doi.org/10.1063/5.0031293>

## INTRODUCTION

The coherent interaction between two resonances at the same energy leads to hybridization and energetic splitting, as is observed, e.g., for coupled resonator modes or molecular orbitals. Facilitating such interaction between excitons and a cavity mode creates light–matter exciton–polaritons and thus enables the tuning of material parameters by light.<sup>1,2</sup> This strong light–matter

coupling has recently been exploited in different organic electronic devices, enabling polariton condensation,<sup>3,4</sup> as well as polariton-based light-emitting diodes,<sup>5</sup> photovoltaic cells,<sup>6</sup> photodiodes,<sup>7</sup> and transistors,<sup>8</sup> among many others. On most of these cases, the device characteristics are made tunable by the hybridization of excitonic and photonic resonances, leading to an enhanced performance if properly employed. In particular, the possible modification of the optical gap and thus the extension of

accessible absorption energies are important for photodetection and photovoltaics.<sup>6</sup>

Semiconducting single-walled carbon nanotubes (SWNTs) exhibit strongly bound excitons with large oscillator strengths at their narrow absorption peaks<sup>9</sup> and are thus ideal candidates to realize strong coupling<sup>10–12</sup> and polaritonic devices<sup>13,14</sup> at room temperature. In addition, the dependence of excitonic absorption on the precise nanotube diameter and (n,m) species<sup>15,16</sup> covers a broad and extremely important spectral range in the near infrared (NIR). Recently, high purity monochiral (6,5) SWNTs<sup>17</sup> have enabled near infrared organic light-emitting diodes<sup>18</sup> and transistors,<sup>13</sup> organic solar cells with low voltage losses,<sup>19</sup> as well as polariton formation<sup>10,11</sup> at wavelengths over 1000 nm. Photodiodes utilizing SWNTs<sup>20–27</sup> hold great potential if strong coupling is successfully employed and promise narrowband, tunable detection wavelengths as hybrid polariton modes can extend the useful absorption toward the red.<sup>7</sup> This approach is fundamentally different from weakly coupled cavity-enhanced photodiodes,<sup>28–31</sup> where a weak absorption has to cover the entire useful spectral range.

In this work, we present the realization of strongly coupled (6,5) SWNT photodetectors with extended and tunable detection wavelengths, shifting the bare  $E_{11}$  absorption from 1000 nm to 1500 nm when hybridized with a cavity mode. We detail two possible realizations of this concept, utilizing either bulk or flat heterojunctions of SWNTs with polymer and fullerene layers and show exciton harvesting of the lower polariton branch (LPB) over an unprecedented range. The addressed spectral detection range is highly suitable for biomedical applications or *in situ* quality assurance in agriculture and industrial manufacturing.

## RESULTS

### Device principle of SWNT photodiodes

Depending on their (n,m) chirality vector, nanotubes can be metallic or semiconducting.<sup>15</sup> Semiconducting SWNTs exhibit a distinct absorption peak for their fundamental excitonic transition,

termed  $E_{11}$ , with the (6,5) SWNTs used in this work showing a strong and narrow absorption peak near 1000 nm. In order to realize a photodiode, these excitons need to be efficiently dissociated at a heterointerface with another material. While the (6,5) SWNTs used in this work are wrapped with PFO-BPy {poly[(9,9-di-n-octylfluorene-2,7-diyl)-alt-(2,2'-bipyridine-6,6'-diyl)]} in the sorting process,<sup>17</sup> the large bandgap and energy levels of this polymer are not suitable to split excitons. Utilizing P3HT (poly[3-hexylthiophene-2,5-diyl]) as a wrapping polymer can introduce a P3HT-donor/SWNT-acceptor junction to generate free charge carriers.<sup>32,33</sup> Care has to be taken as the choice of wrapping polymer can influence the spectral positioning of the absorption lines. Figure 1(a) shows the absorption spectra of PFO-BPy wrapped (6,5) SWNTs peaking at 995 nm, while a partial substitution of PFO-BPy with P3HT leads to a red-shift of their excitonic absorption to 1020 nm.

A full p-i-n diode utilizing P3HT and SWNTs can be realized by the addition of poly(3,4-ethylenedioxythiophene) polystyrene sulfonate (PEDOT:PSS) as hole transport and BPhen:Cs as electron transport layers. Furthermore, a second heterointerface is introduced on the n-side by the addition of PC<sub>70</sub>BM as an electron acceptor,<sup>19,34,35</sup> which does not alter the SWNT absorption further (see [supplementary material](#), Fig. S1). The diode is sandwiched between Au and Ag layers on the hole and electron side of the device, respectively, which act as both electric contacts and cavity mirrors. Figure 1(b) depicts the energy levels of the full device, where excitons are generated on the SWNTs by NIR illumination, are dissociated at either the SWNT-PC<sub>70</sub>BM or SWNT-P3HT interfaces, and the resulting charge carriers are transported to the respective electrodes.

### Tunable strong coupling in SWNTs

Standard organic solar cells and photodetectors require the use of at least one highly transparent contact, such as thin film indium tin oxide (ITO), in order to maximize the amount of light entering the device. Here, the use of metallic contacts instead introduces a strong microcavity effect that can be utilized to selectively enhance specific absorption wavelengths. In the weak coupling regime, a

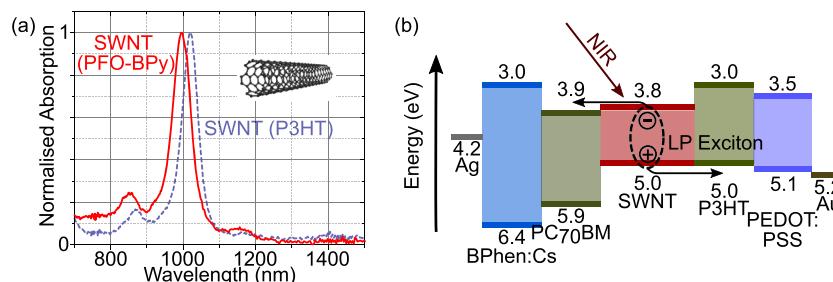


**FIG. 1.** (a) Absorption spectrum of (6,5) single-walled carbon nanotubes (SWNTs) showing a strong  $E_{11}$  exciton absorption peak near 1000 nm. For sorting and stabilization, SWNTs are wrapped in a polymer such as PFO-BPy (red solid line). Changing this polymer can lead to shifts in the absorption wavelength, as demonstrated by a red-shift, when partly exchanging PFO-BPy with P3HT (light blue dashed line). The inset shows the molecular structure of a (6,5) SWNT. (b) Molecular energy levels of a (6,5) SWNTs and the organic materials used and work functions of the metals in the photodiode structure. Exciton-polaritons [lower Polariton (LP) Excitons] are generated by near infrared (NIR) illumination on the SWNTs, and their excitonic component can be dissociated either at the SWNT:PC<sub>70</sub>BM or SWNT:P3HT interfaces. Charges are then transported to their respective contacts by PEDOT:PSS and BPhen:Cs, which act as the hole transport and electron transport material, respectively.

broad and weak absorption can be enhanced by the use of a cavity<sup>29–31</sup> to create narrowband detection. When instead combining a high-quality cavity with a strong excitonic absorber, the system can enter the strong coupling regime. The resulting hybridized exciton–polaritons show an energetic splitting and thus alter the device interaction with external light. Consequently, the optical gap of the material can be manipulated,<sup>6,7</sup> extending the accessible absorption wavelength without chemically altering the absorbing material. We demonstrate that the  $E_{11}$  peak of our SWNTs in the photodiode structure can strongly couple to the cavity mode and, by de-tuning the cavity photon, polaritonic absorption can be shifted by over 300 nm relative to the original exciton peak.

Figure 2(a) shows the angle-resolved excitonic absorption of a reference device comprising a P3HT:PC<sub>70</sub>BM:SWNT mixed layer with only a weak cavity formed by a 90 nm thick ITO and a 100 nm thick Ag contact. Here, the absorption behavior shows no appreciable angular dispersion and is fixed to the  $E_{11}$  exciton peak of the SWNTs. The full linear optical properties of the mixed layer are provided in [supplementary material](#), Fig. S2. Exchanging the ITO contact for a 25 nm thick Au contact leads to the formation of a stronger cavity ( $Q \approx 50$  in the empty cavity) and causes the system to enter the strong coupling regime. Thus, the parabolic cavity mode (black dashed line) and non-dispersive exciton (red dashed line) hybridize and form two polariton states, as depicted in Fig. 2(b). The angle-resolved reflectivity map clearly shows the formation of an upper and lower polariton branch (UPB and LPB) with a distinct energetic splitting. At normal incidence, the original exciton at 1.22 eV splits into an UPB at 1.26 eV and a LPB at 1.19 eV. Fitting the polariton branches in the angle-resolved reflectivity data with a Lorentzian line (see [supplementary material](#), Fig. S3) reveals the angular dispersion of polaritons, which can be modeled by a coupled oscillator Hamiltonian<sup>10</sup> (blue dashed lines), revealing a Rabi splitting of 74 meV in this system.

The formation of polaritonic states depends highly on both the exciton–cavity interaction strength and the position of the cavity mode. Changing the design to a thinner and more highly

concentrated SWNT film while simultaneously utilizing thicker, non-absorbing buffer layers for a strongly red-shifted cavity, we are able to push the LPB down to 0.96 eV and increase the modeled Rabi splitting to 168 meV [Fig. 2(c)]. Here, while the total absorption is similar as in the previous design, a stronger coupling is observed due to the higher concentration of excitons at the anti-node of the optical field in the cavity. Due to the retained hybridization of matter and light, this resonance keeps an excitonic fraction and should thus be able to generate photocurrent,<sup>6,7</sup> even though it is located 260 meV away from the original absorption peak. The polaritonic states in such SWNTs thus clearly provide an opportunity to realize spectrally tunable photodiodes in the near infrared.

### Realization and tuning of strongly coupled SWNT photodiodes

In a p-i-n photodiode, the intrinsic, charge-generating layer can consist of either a bulk heterojunction (BHJ), blending donor, acceptor, and nanotubes in a single layer, or a flat heterojunction (FHJ) structure where a thin SWNT layer is sandwiched between a donor and an acceptor film. As only excitons generated on the SWNTs are of interest, loss of excited states generated by visible light on P3HT and PC<sub>70</sub>BM is acceptable, which enables this flexible design. In the following, we detail and compare both realizations.

Figure 3(a) shows a BHJ-based photodiode structure, comprising a mixed active layer of P3HT:PC<sub>70</sub>BM:SWNT with a variable thickness between 180 nm and 280 nm, a 40 nm thick PEDOT:PSS hole transport layer, and a 50 nm thick BPhen:Cs electron transport layer. A Au bottom contact (25 nm on 1 nm Al) and a Ag top contact (100 nm) form the optical cavity. In this device, the crucial processing step is the deposition of the active layer via spin-coating. Here, sorted (6,5) SWNTs are first washed and then re-dispersed in a P3HT–chlorobenzene solution. PC<sub>70</sub>BM is then added to form the final mixture, which is further processed in inert atmosphere. By varying the concentration of the three solutes, the viscosity of the resulting liquid is strongly altered and must be carefully

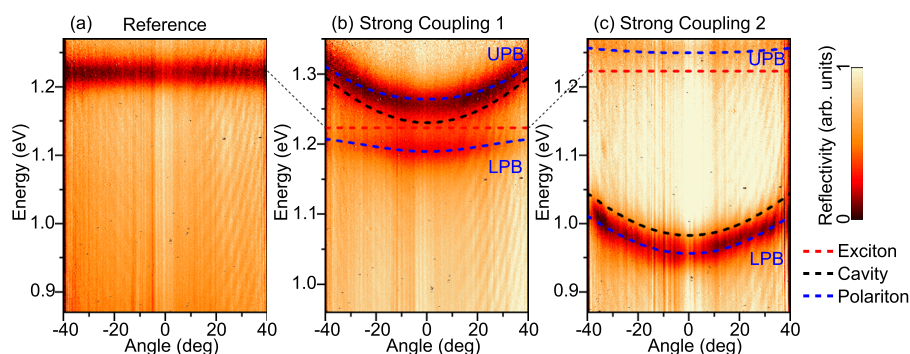


**FIG. 2.** (a)–(c) Angle-resolved reflectivity of SWNT-based devices in false color. (a) Reference device comprising a PC<sub>70</sub>BM:P3HT:SWNT mixed layer in a weak Ag-ITO cavity. A clear absorption dip is seen at the position of the  $E_{11}$  exciton with no angular dispersion. (b) Strongly coupled device comprising a mixed layer with a moderate concentration of SWNTs in an Au–Ag cavity. The formation of polariton branches (dashed blue lines) from the cavity mode (dashed black line) and the exciton (dashed red line) is modeled by a coupled oscillator, showing a Rabi splitting of 74 meV and almost zero detuning between the cavity mode and exciton. The LPB shows an excitonic fraction of 60.0% at 0° incidence. (c) Strongly coupled device comprising a sandwiched SWNT layer with higher concentration than (b) in an Au–Ag cavity, showing a modeled Rabi splitting of 168 meV and a large negative detuning. This leads to a strongly photonic LPB with an exciton fraction of 1.7% at 0° incidence.

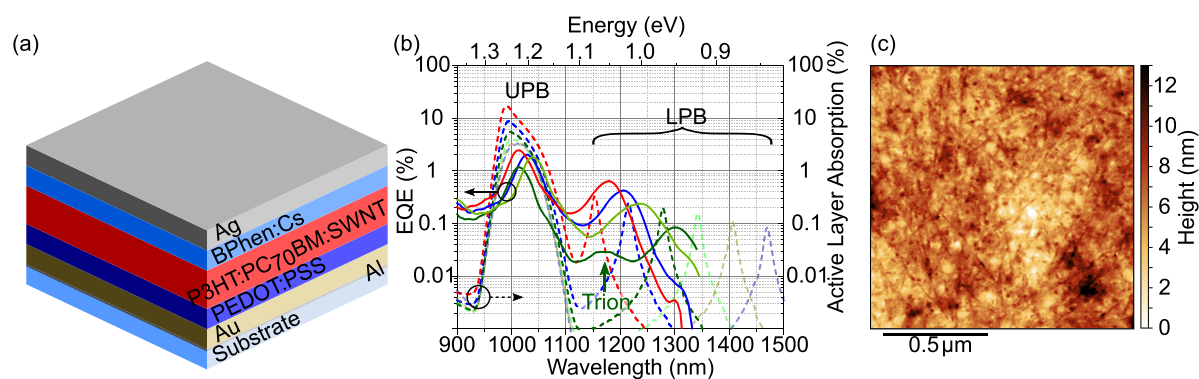


**FIG. 3.** (a) Device schematic for a photodiode employing a P3HT:PC<sub>70</sub>BM:SWNT bulk heterojunction (BHJ), utilizing an Au–Ag cavity with PEDOT:PSS as a hole transport layer and BPhen:Cs as an electron transport layer. SWNTs are wrapped with P3HT and PFO-BPy. (b) Measured external quantum efficiency (EQE, solid lines) and simulated active layer absorption (dashed lines) of BHJ photodiodes with different levels of polariton detuning. By changing the cavity thickness and thus detuning, the resonance of the lower polariton branch (LPB) shifts continuously toward the red, providing a tunable detection wavelength. (c) Atomic force micrograph of the spin coated P3HT:PC<sub>70</sub>BM:SWNT layer. The depicted area shows a root mean square roughness of 1.74 nm.

controlled to achieve a homogeneous film with the desired thickness after spin-coating. Details on this procedure can be found in the Methods section. When the ideal solution parameters are achieved, the thickness of the active layer can be further tuned by a variation of the spin speed, providing the basis for the tuning of the cavity mode.

Figure 3(b) shows the incoming photon-to-electron conversion efficiency or external quantum efficiency (EQE) of the resulting strongly coupled photodiodes under tunable monochromatic illumination without external voltage applied to the device. In the near-infrared spectral region, each device shows two distinct EQE maxima, corresponding to the lower and upper polariton, respectively. Changing the thickness of the mixed layer from 185 nm (red solid line) to 230 nm (dark green solid line) detunes the cavity mode and thus leads to a red-shift of the LPB. We experimentally demonstrate exciton harvesting from the LPB up to 300 nm away from the original absorption and a smooth tunability of the desired photodiode resonance, albeit at only moderate quantum efficiencies. The diode behavior is further confirmed by measuring the current density over the applied voltage [see [supplementary material](#), Fig. S4(a)]. However, the highly conductive SWNTs in the bulk mixed layer lead to a large current in reverse bias, which at  $\pm 2$  V is only one order of magnitude lower than that in the forward direction. This limits the operation of this device type under reverse bias conditions.

In order to assess the possibilities for resonance tuning, we model the active layer absorption with a transfer matrix approach. The dashed lines in Fig. 3(b) show the simulated absorption spectra and provide clear evidence of polariton formation. The main conclusions here are as follows: (i) The simulated absorption is on the same order of magnitude as the measured EQE, suggesting a high internal quantum efficiency despite the low excitonic fraction of the LPB. (ii) The simulated LPB peaks are significantly narrower than the measured EQE. The high viscosity of the SWNT-containing solution leads to a thickness gradient over the  $2 \times 2$  mm<sup>2</sup> device area and hence severely broadens the measured resonance. This behavior could be remedied with different coating methods or additives preventing SWNT aggregation. In addition, scattering by the remaining

SWNT aggregates is likely to play a role in the observed broadening. (iii) The optical simulations suggest that further tuning of the device resonance to 1500 nm and beyond is possible, similar to what has been observed for electroluminescence from strongly coupled (6,5) SWNTs.<sup>13</sup>

In Fig. 3(c), atomic force microscopy of the surface of the mixed P3HT:PC<sub>70</sub>BM:SWNT layer clearly shows SWNTs as long, linear structures embedded in the other organic constituents, explaining the high exciton harvesting efficiency. The mixed layers show only moderate surface roughness (1.74 nm root mean square), suggesting that the broadened detection peaks originate from larger scale inhomogeneities.

As an alternative to the BHJ, SWNTs can be employed as a single thin film sandwiched between donor and acceptor layers in an FHJ. Figure 4(a) shows a schematic of such a device, comprising a thin, highly concentrated SWNT film between 60 nm thick P3HT and PC<sub>70</sub>BM layers. Similar to before, the diode is completed with 25 nm Au on 1 nm Al, 40 nm PEDOT:PSS, 50 nm BPhen:Cs, and 100 nm Ag, as shown in the schematic. The advantage of this design is the use of a thicker, spin-coated acceptor layer on top of the SWNTs in order to prevent both losses through the recombination and reverse current.

The fabrication of this device structure is enabled by the limited solubility of the organic materials in the different solvents. The first P3HT layer is processed from chlorobenzene on top of the PEDOT:PSS. As the P3HT thin film is only poorly soluble in toluene, SWNTs can then be deposited directly from a toluene dispersion. Thin films of SWNTs are practically insoluble unless sonication is applied, enabling subsequent spin-coating of a PC<sub>70</sub>BM film. PC<sub>70</sub>BM is processed from 2-chlorophenol mixed with dichloromethane, which provides high solubility and good surface wetting, respectively, without harming the underlying SWNT and P3HT films.<sup>36</sup>

Figure 4(b) shows the measured EQE of such an FHJ device (solid line), demonstrating two distinct peaks corresponding to the upper and lower polaritons. In addition, transfer matrix calculations are performed (dashed lines), showing further tunability similar to

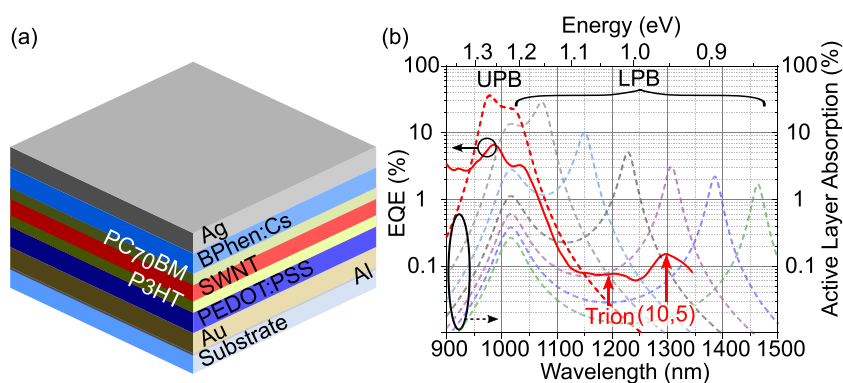


**FIG. 4.** (a) Device schematic for a photodiode utilizing a flat heterojunction (FHJ) of P3HT, SWNTs, and PC<sub>70</sub>BM layers realized by sequential spin-coating. SWNTs are wrapped with PFO-BPy. (b) External quantum efficiency (solid lines) of an FHJ photodiode and simulated absorption spectrum for a 10 nm thick SWNT layer in such a device (dashed lines). The EQE shows distinct upper and lower polariton absorption with possible tunability by varying the P3HT and PC<sub>70</sub>BM layer thicknesses, as demonstrated by the optical simulation. In the measured EQE data, additional low efficiency peaks above 1200 nm indicate absorption by trions as well as the presence of small amounts of larger diameter (10,5) SWNTs.<sup>19</sup>

the BHJ diodes. The EQE in the FHJ photodiode is decreased considerably compared to the optical simulation. We attribute this to excitation loss at the flat junction between SWNTs and donor/acceptor layers and a resulting lower internal quantum efficiency than for the BHJ devices. For the highly concentrated SWNT films, thickness and SWNT concentration strongly depend on processing conditions, leading to inaccuracies when comparing the optical simulation with a real device. Nevertheless, the transfer matrix model indicates that if the generated excitons can be properly harvested, efficiencies of several percent are possible over an extended tunability range of 500 nm.

The diode behavior shown in Fig. S4(b) (supplementary material) shows a clear improvement over the BHJ case, with a reduction in reverse current by an order of magnitude. Consequently, the thermal noise current generated in this device improves considerably. By considering only shot and thermal noise,<sup>31,37</sup> we determine a lower limit for the noise current of  $> 8 \times 10^{-13} \text{ A}/\sqrt{\text{Hz}}$  at short circuit. This reveals an upper limit for the specific detectivity<sup>38</sup> in this device on the order of Jones, further depending on the operating frequency (for more details, see supplementary material, note 1). Future improvements will have to target both the EQE by increasing the SWNT concentration and internal quantum efficiency as well as the reduction of reverse and noise currents.

## DISCUSSION

We have demonstrated near-infrared polariton photodiodes based on strong light-matter coupling of (6,5) SWNT excitons with a metal cavity. By utilizing strong negative detuning of the photonic mode, the hybridized detection peak related to the LPB can be continuously shifted toward the red, from 1000 nm to over 1500 nm, while still providing photocurrent in the device. We have shown realizations of this principle based on both bulk and flat heterojunction architectures, obtaining photodiodes with tunable strong coupling. For the BHJ devices, we have created a novel blend film of P3HT, PC<sub>70</sub>BM, and SWNTs, with high exciton harvesting efficiencies and a broad distribution of nanotubes in a thick active film. In

turn, we demonstrated spectrally tunable photocurrent generation from the lower polariton branch of the device up to a wavelength of 1300 nm. Alternatively, by sequentially depositing the donor, SWNTs, and the acceptor, we realized an FHJ structure, enabling an improved diode behavior. The presented results showcase the large application potential of polariton-based SWNT photodiodes for tunable near infrared photodetection beyond the band edge of silicon. The working principle shown here may be applied to higher nanotube chiralities to extend the spectral range even further. Future research will address processability, focusing on smoother and more homogeneous film formation for which we expect drastic improvements in device performance.

## METHODS

### SWNT sorting

As described previously,<sup>17</sup> (6,5) SWNTs were selectively extracted from the CoMoCAT raw material (Chasm Advanced Materials, SG65i-L58, 0.38 g/L) by shear force mixing (Silverson L2/Air, 10 230 rpm, 72 h) and polymer-wrapping with PFO-BPy (American Dye Source,  $M_w = 40 \text{ kg/mol}$ , 0.5 g/l) in toluene. Aggregates were removed by centrifugation at 60 000 g (Beckman Coulter Avanti J26XP centrifuge) for  $2 \times 45 \text{ min}$  with intermediate supernatant extraction.

### Preparing the P3HT:PC<sub>70</sub>BM:SWNT solution

The (6,5) SWNT dispersion was passed through a PTFE membrane filter (Merck Millipore, JVWP, 0.1  $\mu\text{m}$  pore size). The resulting film was washed twice with toluene for 10 min at 80 °C to reduce the PFO-BPy content. SWNTs were then re-dispersed at 0.5 g/l in a solution of chlorobenzene with regio-regular poly(3-hexylthiophene-2,5-diyl) (P3HT, BASF SE,  $M_w = 64 \text{ kg/mol}$ , 3.5 g/l) and ultrasonicated until homogeneous ( $\sim 2 \text{ h}$ ). To this solution, [6,6]-Phenyl-C<sub>71</sub>-butyric acid methyl ester (PC<sub>70</sub>BM > 99%, Lumtec) was added in a concentration of 4 g/l and sonicated until

homogeneous. During ultrasonication, the bath (Branson 2800 MH Ultrasonic Cleaner) and solution were actively cooled to remain at room-temperature.

### Sample fabrication

Glass substrates were cleaned by ultrasonication with acetone, 2-propanol, and de-ionized water for 10 min each and subsequently treated by  $O_2$  plasma for 3 min. 1 nm Al (as seed layer) and 25 nm Au were deposited by thermal evaporation in a vacuum chamber (Angstrom EvoVac) at a base pressure of  $1 \times 10^{-7}$  mbar. Samples were taken out of the chamber and treated again with  $O_2$  plasma to create a hydrophilic surface. Poly(3,4-ethylenedioxythiophene) polystyrene sulfonate (PEDOT:PSS, P VP AI4083, Clevios) was spin-coated at 3000 rpm to form a 40 nm layer and annealed at  $150^\circ\text{C}$  for 10 min. After annealing, substrates were immediately transferred to a dry nitrogen glovebox. For the BHJ device, the prepared P3HT:PC<sub>70</sub>BM:SWNT solution was spin-coated from chlorobenzene at speeds between 500 rpm and 2000 rpm. For the FHJ device, P3HT was dissolved in chlorobenzene (14 g/l) and spin-coated at 2000 rpm–2500 rpm after filtration to form an  $\approx 60$  nm thick film. SWNTs were re-dispersed in toluene (0.5 g/l) by ultrasonication and spin-coated at 1000 rpm. PC<sub>70</sub>BM was dissolved in dichloromethane:2-chlorophenol (1:1) at a concentration of 20 g/l and spin-coated at 2000 rpm–2500 rpm to form an  $\approx 60$  nm thick film. To finish both BHJ and FHJ devices, 50 nm 4,7-diphenyl-1,10-phenanthroline (BPhen) doped with Cs as a hole transport layer and 100 nm Ag as a top electrode/mirror were deposited by thermal evaporation in the vacuum chamber as mentioned above. Finished devices were encapsulated with a glass lid and moisture getter using a UV-curable epoxy (Norland NOA68). The device active area was  $4.0\text{ mm}^2$ .

### EQE and jV measurement

Device current density–voltage characteristics were recorded with a source measuring unit (SMU, Keithley 2450) supplying voltage and measuring current. External quantum efficiency measurements were performed by measuring photocurrent at 0 V (short-circuit current) under illumination by a tunable (1 nm linewidth) optical parametric amplifier (Ekspla PG403) pumped by using a diode-pumped solid-state regenerative amplifier laser (Ekspla PL2210) focused onto the measured active area. Input optical power was adjusted using neutral density filters and calibrated to 0.1 mW over the measured spectral range by amplified Si (Thorlabs PDA100A) and Ge (Thorlabs PDA50B2) photodiodes. The calculated EQE spectra were smoothed over 5 nm using a Savitzky–Golay algorithm.

### Optical characterization

Absorption and spectroscopic ellipsometry measurements of single layers of SWNT and P3HT:PC<sub>70</sub>BM:SWNT were performed using a variable angle spectroscopic ellipsometer (VASE, M2000, J.A. Woollam), and optical constants were modeled using the CompleteEASE software (J.A. Woollam). For angle-resolved reflectivity measurements, a white light source (Ocean Optics, HL-2000-FHSA) was focused onto the sample by an infinity corrected 50 $\times$  NIR objective with 0.65 NA (Olympus, LCPLN50XIR). The resulting

spot diameter of  $\approx 4\ \mu\text{m}$  defined the investigated area on the sample. The reflected light from the sample was imaged from the back focal plane of the objective onto the entrance slit of a spectrometer (Princeton Instruments IsoPlane SCT 320) using a 4f Fourier imaging system ( $f_1 = 20\text{ mm}$  and  $f_2 = 300\text{ mm}$ ). A linear polarizer was placed in front of the spectrometer to select between TE and TM polarization. The layer thicknesses of investigated samples can be approximated as follows. *Reference*: 90 nm ITO | 40 nm PEDOT:PSS | 160 nm P3HT:PC<sub>70</sub>BM:SWNT blend | 50 nm BPhen:Cs | 100 nm Ag. *Strong coupling 1*: 25 nm Au|40 nm PEDOT:PSS | 160 nm P3HT:PC<sub>70</sub>BM:SWNT blend | 50 nm BPhen:Cs | 100 nm Ag. *Strong coupling 2*: 25 nm Au | 40 nm PEDOT:PSS | 95 nm P3HT |  $\approx 10$  nm SWNT | 95 nm PC<sub>70</sub>BM | 50 nm BPhen:Cs | 100 nm Ag.

### Modeling

Polariton branches are modeled from the measured reflectivity maps by peak-fitting the reflectivity dips and subsequently fitting a coupled oscillator model<sup>10</sup> to the measured dispersion with the cavity mode, Rabi splitting, and effective refractive index as free parameters. Active layer absorption is modeled using a transfer matrix approach, as in the study of Burkhard *et al.*,<sup>39</sup> using the optical constants determined from ellipsometry.

### Atomic force microscopy

Atomic force microscope images were obtained using a Dimension Icon (Bruker Co.) atomic force microscope in the ScanAsyst mode.

### SUPPLEMENTARY MATERIAL

The [supplementary material](#) showing the absorption spectra of wrapped SWNTs, optical constants of the P3HT:PC<sub>70</sub>BM:SWNT blend film, Lorentzian fitting of reflectivity spectra, jV characteristics of the demonstrated photodiodes, and a description of the estimation of the specific detectivity is available.

### ACKNOWLEDGMENTS

The authors gratefully acknowledge funding from the Volkswagen Foundation within Project No. 93404. A.M. acknowledges further funding through an individual fellowship of the Deutsche Forschungsgemeinschaft (Grant No. 404587082).

### DATA AVAILABILITY

The data that support the findings of this study are openly available in the St Andrews Research Portal at <https://doi.org/10.17630/8241bbe7-274d-4204-8ed0-af108802e88f>.<sup>40</sup>

### REFERENCES

- 1 K. Stranius, M. Hertzog, and K. Börjesson, “Selective manipulation of electronically excited states through strong light-matter interactions,” *Nat. Commun.* **9**, 2273 (2018).
- 2 R. F. Ribeiro, L. A. Martínez-Martínez, M. Du, J. Campos-Gonzalez-Angulo, and J. Yuen-Zhou, “Polariton chemistry: Controlling molecular dynamics with optical cavities,” *Chem. Sci.* **9**, 6325–6339 (2018).

- <sup>3</sup>J. D. Plumhof, T. Stöferle, L. Mai, U. Scherf, and R. F. Mahrt, "Room-temperature Bose-Einstein condensation of cavity exciton-polaritons in a polymer," *Nat. Mater.* **13**, 247 (2014).
- <sup>4</sup>K. S. Daskalakis, S. A. Maier, R. Murray, and S. Kéna-Cohen, "Nonlinear interactions in an organic polariton condensate," *Nat. Mater.* **13**, 271–278 (2014).
- <sup>5</sup>A. Genco *et al.*, "Bright polariton coumarin-based OLEDs operating in the ultrastrong coupling regime," *Adv. Opt. Mater.* **6**, 1800364 (2018).
- <sup>6</sup>V. C. Nikolis *et al.*, "Strong light-matter coupling for reduced photon energy losses in organic photovoltaics," *Nat. Commun.* **10**, 3706 (2019).
- <sup>7</sup>E. Eizner, J. Brodeur, F. Barachati, A. Sridharan, and S. Kéna-Cohen, "Organic photodiodes with an extended responsivity using ultrastrong light-matter coupling," *ACS Photonics* **5**, 2921–2927 (2018).
- <sup>8</sup>A. V. Zasedatelev *et al.*, "A room-temperature organic polariton transistor," *Nat. Photonics* **13**, 378–383 (2019).
- <sup>9</sup>F. Wang, "The optical resonances in carbon nanotubes arise from excitons," *Science* **308**, 838–841 (2005).
- <sup>10</sup>A. Graf, L. TROPF, Y. Zakharko, J. Zaumseil, and M. C. Gather, "Near-infrared exciton-polaritons in strongly coupled single-walled carbon nanotube microcavities," *Nat. Commun.* **7**, 13078 (2016).
- <sup>11</sup>W. Gao, X. Li, M. Bamba, and J. Kono, "Continuous transition between weak and ultrastrong coupling through exceptional points in carbon nanotube microcavity exciton-polaritons," *Nat. Photonics* **12**, 362–367 (2018).
- <sup>12</sup>Y. Zakharko, A. Graf, and J. Zaumseil, "Plasmonic crystals for strong light-matter coupling in carbon nanotubes," *Nano Lett.* **16**, 6504–6510 (2016).
- <sup>13</sup>A. Graf *et al.*, "Electrical pumping and tuning of exciton-polaritons in carbon nanotube microcavities," *Nat. Mater.* **16**, 911–917 (2017).
- <sup>14</sup>C. Möhl *et al.*, "Trion-polariton formation in single-walled carbon nanotube microcavities," *ACS Photonics* **5**, 2074–2080 (2018).
- <sup>15</sup>X. Wei *et al.*, "Experimental determination of excitonic band structures of single-walled carbon nanotubes using circular dichroism spectra," *Nat. Commun.* **7**, 12899 (2016).
- <sup>16</sup>R. B. Weisman and S. M. Bachilo, "Dependence of optical transition energies on structure for single-walled carbon nanotubes in aqueous suspension: An empirical Kataura plot," *Nano Lett.* **3**, 1235–1238 (2003).
- <sup>17</sup>A. Graf *et al.*, "Large scale, selective dispersion of long single-walled carbon nanotubes with high photoluminescence quantum yield by shear force mixing," *Carbon* **105**, 593–599 (2016).
- <sup>18</sup>A. Graf, C. Murawski, Y. Zakharko, J. Zaumseil, and M. C. Gather, "Infrared organic light-emitting diodes with carbon nanotube emitters," *Adv. Mater.* **30**, 1706711 (2018).
- <sup>19</sup>A. Classen *et al.*, "Absence of charge transfer state enables very low  $V_{OC}$  losses in SWCNT: Fullerene solar cells," *Adv. Energy Mater.* **9**, 1801913 (2019).
- <sup>20</sup>R. M. Jain *et al.*, "Polymer-free near-infrared photovoltaics with single chirality (6,5) semiconducting carbon nanotube active layers," *Adv. Mater.* **24**, 4436–4439 (2012).
- <sup>21</sup>A.-M. Dowgiallo, K. S. Mistry, J. C. Johnson, and J. L. Blackburn, "Ultrafast spectroscopic signature of charge transfer between single-walled carbon nanotubes and  $C_{60}$ ," *ACS Nano* **8**, 8573–8581 (2014).
- <sup>22</sup>T. A. Shastry and M. C. Hersam, "Carbon nanotubes in thin-film solar cells," *Adv. Energy Mater.* **7**, 1601205 (2017).
- <sup>23</sup>J. L. Blackburn, "Semiconducting single-walled carbon nanotubes in solar energy harvesting," *ACS Energy Lett.* **2**, 1598–1613 (2017).
- <sup>24</sup>Y. Liu, J. Zhang, H. Liu, S. Wang, and L.-M. Peng, "Electrically driven monolithic subwavelength plasmonic interconnect circuits," *Sci. Adv.* **3**, e1701456 (2017).
- <sup>25</sup>D. J. Bindl, M. J. Shea, and M. S. Arnold, "Enhancing extraction of photogenerated excitons from semiconducting carbon nanotube films as photocurrent," *Chem. Phys.* **413**, 29–34 (2013).
- <sup>26</sup>D. J. Bindl, M.-Y. Wu, F. C. Prehn, and M. S. Arnold, "Efficiently harvesting excitons from electronic type-controlled semiconducting carbon nanotube films," *Nano Lett.* **11**, 455–460 (2011).
- <sup>27</sup>M. S. Arnold *et al.*, "Broad spectral response using carbon nanotube/organic semiconductor/ $C_{60}$  photodetectors," *Nano Lett.* **9**, 3354–3358 (2009).
- <sup>28</sup>S. Liang *et al.*, "Microcavity-integrated carbon nanotube photodetectors," *ACS Nano* **10**, 6963–6971 (2016).
- <sup>29</sup>K. Kishino *et al.*, "Resonant cavity-enhanced (RCE) photodetectors," *IEEE J. Quantum Electron.* **27**, 2025–2034 (1991).
- <sup>30</sup>A.-K. Kishino *et al.*, "Resonant cavity enhanced (RCE) photodetectors," in *Instrumentation in the Aerospace Industry: Proceedings of the International Symposium* (Instrument Society of America, 1998), Vol. 44, pp. 479–487.
- <sup>31</sup>B. Siegmund *et al.*, "Organic narrowband near-infrared photodetectors based on intermolecular charge-transfer absorption," *Nat. Commun.* **8**, 15421 (2017).
- <sup>32</sup>T. Schuettfort, A. Nish, and R. J. Nicholas, "Observation of a type II heterojunction in a highly ordered polymer-carbon nanotube nanohybrid structure," *Nano Lett.* **9**, 3871–3876 (2009).
- <sup>33</sup>S. D. Stranks *et al.*, "Ultrafast charge separation at a polymer—Single-walled carbon nanotube molecular junction," *Nano Lett.* **11**, 66–72 (2011).
- <sup>34</sup>T. A. Shastry *et al.*, "Enhanced uniformity and area scaling in carbon nanotube-fullerene bulk-heterojunction solar cells enabled by solvent additives," *Adv. Energy Mater.* **6**, 1501466 (2016).
- <sup>35</sup>D. J. Bindl, A. S. Brewer, and M. S. Arnold, "Semiconducting carbon nanotube/fullerene blended heterojunctions for photovoltaic near-infrared photon harvesting," *Nano Res.* **4**, 1174–1179 (2011).
- <sup>36</sup>F. Machui, S. Langner, X. Zhu, S. Abbott, and C. J. Brabec, "Determination of the P3HT:PCBM solubility parameters via a binary solvent gradient method: Impact of solubility on the photovoltaic performance," *Sol. Energy Mater. Sol. Cells* **100**, 138–146 (2012).
- <sup>37</sup>R. D. Jansen-van Vuuren, A. Armin, A. K. Pandey, P. L. Burn, and P. Meredith, "Organic photodiodes: The future of full color detection and image sensing," *Adv. Mater.* **28**, 4766–4802 (2016).
- <sup>38</sup>R. C. Jones, "Proposal of the detectivity  $D^{**}$  for detectors limited by radiation noise," *J. Opt. Soc. Am.* **50**, 1058 (1960).
- <sup>39</sup>G. F. Burkhard, E. T. Hoke, and M. D. McGehee, "Accounting for interference, scattering, and electrode absorption to make accurate internal quantum efficiency measurements in organic and other thin solar cells," *Adv. Mater.* **22**, 3293–3297 (2010).
- <sup>40</sup>A. Mischock *et al.* (2020). "Spectroscopic near-infrared photodetectors enabled by strong light-matter coupling in (6,5) single-walled carbon nanotubes," St. Andrews Research Portal, Dataset. <https://doi.org/10.17630/8241bbe7-274d-4204-8ed0-af108802e88f>.